

Opinion

Old Discovery Leading to New Era: Metabolic Imaging of Cancer with Deuterium MRI

Hao Ding ^{1,*} , Athar Haroon ², Simon Wan ³, Thoralf Niendorf ^{4,5}  and Sola Adeleke ^{6,7} ¹ School of Medicine, Imperial College London, London SW7 2AZ, UK² Department of Nuclear Medicine, Barts Health NHS Trust, London SE5 9RS, UK³ Institute of Nuclear Medicine, University College London, London WC1E 6BT, UK⁴ Charité—Berlin University of Medicine, Corporate Member of Freie Universität Berlin and Humboldt Universität zu Berlin, 10587 Berlin, Germany⁵ Berlin Ultrahigh Field Facility (B.U.F.F.), Max-Delbrueck Center for Molecular Medicine in the Helmholtz Association, 13125 Berlin, Germany⁶ Department of Oncology, Guy's and St Thomas' NHS Foundation Trust, London SE1 9RT, UK⁷ School of Cancer & Pharmaceutical Sciences, King's College London, London WC2R 2LS, UK

* Correspondence: hd919@ic.ac.uk

Abstract: The understanding of metabolic compartments involved in the survival, growth and invasion of tumours is important for modern cancer research. Deuterium metabolic spectroscopy (DMS) and metabolic imaging (DMI) have been demonstrated as robust, straightforward tools for visualising tumour metabolism *in vivo*. However, for them to become part of the cancer patient's management pathway in a clinical setting, there remain many obstacles to overcome. Technological advancement in magnetic resonance imaging hardware and processing is needed. Further justification of DMI's potential also requires more human study and multidisciplinary collaboration.

Keywords: deuterium; metabolic spectroscopy; metabolic imaging; cancer



Citation: Ding, H.; Haroon, A.; Wan, S.; Niendorf, T.; Adeleke, S. Old Discovery Leading to New Era: Metabolic Imaging of Cancer with Deuterium MRI. *Magnetochemistry* **2023**, *9*, 6. <https://doi.org/10.3390/magnetochemistry9010006>

Academic Editor: Serge Smirnov

Received: 14 November 2022

Revised: 16 December 2022

Accepted: 22 December 2022

Published: 25 December 2022



Copyright: © 2022 by the authors. Licensee MDPI, Basel, Switzerland. This article is an open access article distributed under the terms and conditions of the Creative Commons Attribution (CC BY) license (<https://creativecommons.org/licenses/by/4.0/>).

1. Introduction

The understanding of metabolic pathways leading to tumour formation is of fundamental importance for modern cancer research. Tumour cells utilise nutrients such as glucose to produce adenosine 5'-triphosphate (ATP) at much higher rates than normal body cells [1] because malignant cells need more energy for aggressive proliferation. Variable molecules synthesised or consumed by tumour cells are potential biomarkers if their concentrations differ from that of normal body cells [1]. Change in biomarker level could indicate tumour progression or regression and thus has potential to be a monitoring tool. Complex metabolic processes involved in the survival, growth and invasion of tumours can also be the target of novel anti-cancer therapy.

In current clinical settings, positron-emission tomography (PET) technique is the standard of care for studying the uptake of glucose in patient's body via ¹⁸F-fluorodeoxyglucose (FDG) injection. However, ¹⁸F-FDG-PET is affected by several factors including altered blood glucose levels, duration of fasting, muscle activation such as exercise and steroids [2]. Radiation exposure during the PET scan also limits the frequency of tumour assessment before and after cancer treatments [3]. In recent years, magnetic resonance spectroscopy (MRS) has gained popularity in research due to its non-ionising nature and can be a powerful tool for monitoring metabolic processes non-invasively. Proton magnetic resonance spectroscopic imaging (MRSI) can map metabolite concentrations but is unable to dynamically describe over time, the activity of metabolic pathways [4]. Dynamic ¹³C MRS following the injection of hyperpolarized ¹³C-enriched substrates is a powerful method for determining metabolic fluxes accurately *in vivo* [5]. However, this technique requires polarization to happen on-site and close to the scanner, which increases the expense, and it is technically demanding [6].

Recently, deuterium (^2H) metabolic spectroscopy (DMS) and metabolic imaging (DMI) have been demonstrated as more straightforward alternatives to ^{13}C MRS for imaging of tumour metabolism *in vivo* [7–9]. This article aims to explain the unique advantage of DMS and DMI, summarize and comment on the latest studies using DMI for cancer metabolic assessment and monitoring. Outlook and potential challenges for DMI's clinical integration are also discussed to inspire and guide further research.

2. Development and Principle of DMS and DMI

The discovery of mass-2 hydrogen isotope was made by Urey et al. in 1931, who named it deuterium two years later [10]. In 1987, ^2H MRS was developed with deuterated water as a tracer to measure blood flow and tissue perfusion; its potential for metabolism study was also briefly discussed [11]. In the same year, the first deuterium-based magnetic resonance imaging (MRI) experiment was described by Muller and Seelig who mapped the inflow of deuterated water in rat's brains [12].

These early studies showed some favourable features of ^2H nuclear magnetic resonance (NMR). ^2H has a low natural abundance of 0.0115% [13] and does not require water suppression or outer volume suppression to exclude lipid tissue contaminating signals. The low ^2H Larmor frequency [14] means ^2H MRS is minimally affected by magnetic field inhomogeneity. Furthermore, ^2H generates a large quadrupolar magnetic moment which leads to relatively short T_1 and T_2 relaxation times. These relaxation properties favour rapid scanning which enhances the sensitivity of ^2H MRI for brain applications by outer volume suppression [11,12].

In 2017, Lu et al. [8] demonstrated DMS for the first time with deuterated glucose ($[6,6'\text{-}^2\text{H}_2]$ glucose) as tracer to study rat brain metabolism at a magnetic field strength of 16.4 T. After deuterated glucose is taken up in cells, $[^2\text{H}]$ -labelling is firstly incorporated into pyruvate through glycolysis [15]. Under aerobic conditions, pyruvate turns into $[2,2\text{-}^2\text{H}]$ acetyl coenzyme A in mitochondria, catalysed by pyruvate dehydrogenase. Labelled acetyl coenzyme A enters tricarboxylic acid cycle and produce intermediates such as alpha-ketoglutarate which consequently lead to production of $[4,4'\text{-}^2\text{H}_2]$ -glutamate and $[4,4'\text{-}^2\text{H}_2]$ -glutamine. From the tricarboxylic acid cycle, $[^2\text{H}]$ -labelling can exchange with the protons in water molecules to generate labelled water. Labelled-pyruvate can also be metabolized to $[3,3\text{-}^2\text{H}]$ -lactate anaerobically, catalysed by lactate dehydrogenase. Therefore, Lu et al. [8] were able to monitor dynamic changes of labelled glucose, glutamate + glutamine (Glx) and water contents in the brain and obtain dynamic DMS in just 15 s (0.3 s repetition time (TR) with 50 averages). The data can be translated to quantitative values with metabolic modelling for metabolic pathway fluxes such as tricarboxylic acid cycle.

Soon following the demonstrations of DMS, Feyter et al. [7] tested the idea of DMI and non-invasively generated steady-state metabolic maps to show the metabolic fate of several ^2H -labeled substrates (Figure 1) [9]. According to Warburg effect, instead of oxidative glucose metabolism like in normal tissue, tumour cells shift to glycolytic metabolism in the presence of sufficient oxygen [16]. Tracking of lactate and Glx can generate a Warburg effect (Lac/Glx) map and was used in the study of De Feyter et al. [7] to show pronounced metabolic differences between tumour and normal tissue.

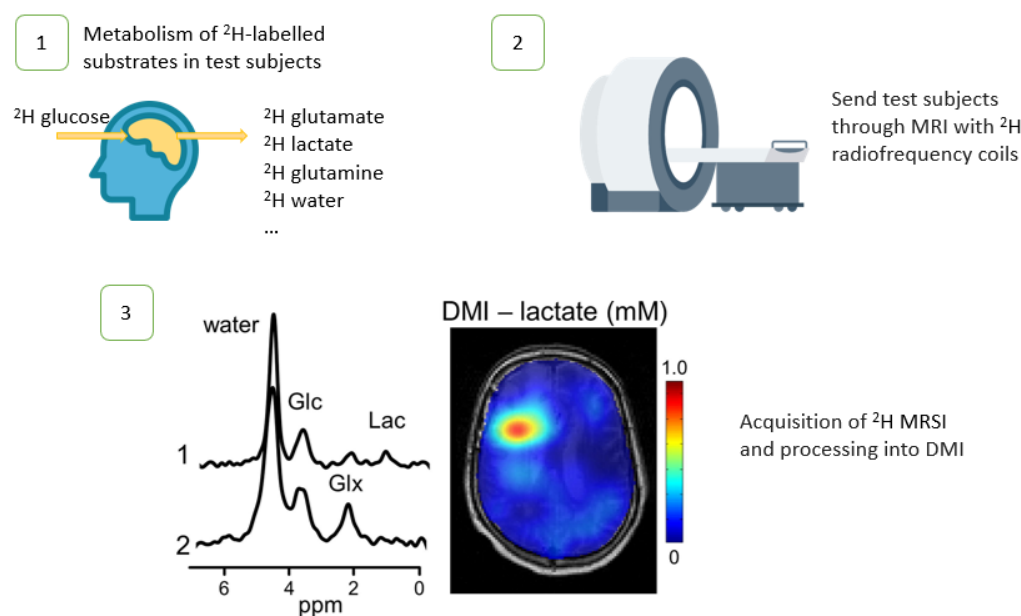


Figure 1. Workflow of a DMI study: Deuterated substrate can be administered orally or intravenously. Substrate is metabolised in the cells to downstream products while the test subject relaxes outside the MRI, or inside the MRI if there is an interest to follow the formation of metabolic products over time. Consequently, DMI data is generated by quantification of the deuterium spectra at each spatial location by spectral fitting [9].

3. In Vivo Tumour Detection Using DMI

Since DMI was first introduced in 2018, its application in cancer research is still at an early preclinical stage with most experiments carried out in rodent models only. Different tumour subtypes can be induced in mice and thus, provide sufficient evidence as proof-of-concept studies and are the only feasible method for testing the utility and safety of deuterium labelled compounds.

De Feyter et al. [7] investigated brain tumours in their pioneer study. Since then, DMI has also been used to investigate other types of cancer. Markovic et al. [17] induced pancreatic ductal adenocarcinoma (PDAC) in mice with two different mutations to mimic the diversity of human pancreatic cancer aetiology. The DMI acquisitions were carried out with slice-selective 2D chemical-shift imaging (CSI) and a repetition time of 95 ms. For both models, DMI detected the presence of the tumours bigger than 5mm due to the generation of deuterated lactate. However, the ability to detect smaller tumour is limited by the nominal in-plane resolution of 5 mm. No significant difference was observed between the rates of glucose to lactate conversion in two tumour models. Markovic et al. [17] consequently developed a kinetic model that describes the dynamic change of the metabolites. The statistically different clearance rates of lactate and glucose obtained from the two models can help to distinguish their unique vasculatures. This study highlighted the potential of DMI for tumour characterisation, but also the need for higher spatial resolution for visualisation of heterogeneities in glucose uptake and in lactate production. Recognizing this opportunity, Peters et al. implemented a multi-echo balanced steady-state free precession (ME-bSSFP) approach to enhance signal-to-noise ratio of DMI versus a CSI based approach while achieving spectral isolation of the metabolic precursors and products. DMI with ME-bSSFP at 15.2 T enabled an increase in spatial resolution of 16 versus CSI based DMI and facilitated imaging of lactate generated in a transgenic mouse model of pancreatic ductal adenocarcinoma [18]. A sensitivity gain was also achieved in 3D DMI although the scanning time is significantly longer versus 2D acquisitions. Veltien et al. [19] performed 3D DMI for renal tumours in mice at 11.7 T field and was able to obtain high nominal resolution of 8 μ L in 37 min. A lower resolution around 50 μ L was achieved in 24 min.

Other than glucose metabolism, increased choline uptake is another hallmark of tumour development [20]. In this early feasibility study, it was demonstrated that the deuterated choline and glucose signals are well separated in a ^2H MR spectrum of an $8\ \mu\text{L}$ voxel in the DMI and they also observed a resolved signal for deuterated lactate. It is worth noticing that the averaged tissue concentrations of [^2H] choline over the time course of DMI accumulated in different tumours are different with variable spatial distributions. It is possible that when more labelled substrates are seen, metabolic heterogeneities are more likely to be observed to aid future characterisation of tumours. For these progresses to have an impact in clinical settings, similar experiments should be carried out at a clinical magnetic field strength, i.e., 3T. To apply DMI of choline and glucose at lower field strengths, their signals need to be resolved from each other. Veltien et al. [19] hypothesized that glucose and choline signals can be distinguished at 7 T with sufficient spectral separation. At 3 T distinguishability for instance may depend on magnetic field shimming conditions, although time difference between different signals appearances should also be considered. Testing this hypothesis warrants further research.

4. In Vivo Treatment Response Monitoring Using DMI

DMS and DMI not only hold potential for tumour identification and characterisation, understanding of cancer metabolism can also contribute to treatment monitoring. For most solid tumours, the current clinical standard for treatment response evaluation is measurement of tumour size using computed tomography (CT) or MRI [21]. Early stage molecular response usually happens quicker following treatment than morphological changes and might more accurately reflect tumour regression [22]. Therefore, imaging techniques that can detect biomarkers of cancer response are of great interest for assessing treatment efficacy, optimizing personalised medicine, and reducing the burden of unnecessary treatments

Measurements of ^2H labelled fumarate conversion to ^2H -labeled malate can be used to detect tumor cell death, as demonstrated by the in vivo study from Hesse et al. [23]. DMI at 7 T could detect the increase in malate production in necrotic tumour tissue. The malate/fumarate ratio increased more than 10 folds in murine lymphoma, human breast and colorectal xenografts after drug treatment and was correlated with increased levels of tumour cell death measured in excised tumor sections. Similar results can be obtained using ^{13}C MRS [24]. However, since the DMI technique does not require a hyperpolarizer, it is a less expensive option. For possible future clinical implementation, detection of fumarate and malate at 3 T should be tested and the safe dosage of fumarate needs further investigation. A recently published study by Taglang et al. [25] explored the link between glycolytic flux in tumour cells and relevant genetic pathway in more detail with DMS. Telomeres are protective structures at the ends of cell chromosomes and cancer cells often have genetic mutations to maintain telomere length for uncontrolled proliferation. Taglang et al. [25] identified a mechanistic link between telomere maintenance and elevated glycolysis in astrocytoma models. The exact pathway is beyond the scope of this article, however, they provided a more fundamental explanation to the importance of monitoring glucose flux to lactate, instead of steady-state lactate, for accurate astrocytoma progression monitoring which is challenging for conventional MRI [26]. Furthermore, with DMS they were able to demonstrate that [6,6'- ^2H]-glucose flux to lactate is reduced following cancer treatment and DMI enables visualization of treatment induced tumour lesion that cannot be distinguished from tumour by standard MRI.

Telomere maintenance is determined by more than one genetic pathway so, more potential tags exist than just [6,6'- ^2H]-glucose. Batsios et al. [27] evaluated the utility of [U- ^2H]-pyruvate as a DMI agent after establishing the mechanism of another pathway for telomere maintenance. Even when clinically feasible MRI field strength of 3 T was applied, significant reduction in [U- ^2H]-pyruvate metabolism to lactate can be observed at day 5 ± 2 following chemotherapy treatment, prior to tumour volume shrinkage. This suggests early potential promise for clinical translation.

5. Future Perspectives for Clinical Implementation and Challenges

Preclinical studies summarized above have highlighted the potential of DMS and DMI for cancer research. For them to be integrated into clinical setting and become part of the cancer patient's management pathway, there remains many steps and challenges to overcome. We hereby suggest a few directions that future research might focus on.

1. Identifying more biomarkers: Deuterated glucose was the first and commonly injected label for DMS and DMI study. However, as demonstrated by other recent studies [25,27], identification of other appropriate biomarkers and thorough understanding of their journey through relevant metabolic pathways is crucial for DMI to become a powerful tool in cancer management. Adoption of strategies described in the imaging biomarker development roadmap [28] should provide guidance on a robust translational path and ensure clinical adoption based on the quality of evidence generated from clinical studies [29]. Even if some biomarkers become unsuccessful for clinical translation, they could still be valuable in basic and translational research for monitoring metabolic pathways that novel treatment agents could target. Other ^2H -labeled tracers that might be taken into consideration include but not limited to acetate, fumarate, succinate . . . [30].
2. Imaging optimisation: Early preclinical studies should further refine and improve DMI acquisition techniques to provide an effective and technically achievable method to be used in subsequent clinical trials. Dynamic DMI measurements of $[6,6' - ^2\text{H}_2]$ -labelled glucose with a high temporal (10 min) and spatial resolution (2.96 mL) of healthy human brain is achievable as demonstrated by Ruhm et al. [31] However, the dedicated coil design and the ultrahigh field strength of 9.4 T make the setting less available routinely in a hospital. The sensitivity of MRI and MRS improves with higher magnetic fields [32,33] but there are other optimization methods to mitigate this requirement. De Graaf et al. [34] showed that with optimal multi-receiver arrays, a nominal 1 mL resolution DMI acquisition is feasible at 7 T and proposed that clinical use field strength of 3 T should allow for a nominal 4–8 mL DMI acquisition. Kaggie et al. [35] attempted taking DMI of human brain at 3 T for the first time recently. Although there was spectral overlap between metabolites, their DMS was able to distinguish metabolic peaks corresponding to water, glucose, Glx, and lactate. Other techniques such as multi-echo balanced steady-state free precession instead of CSI [18] or deployment of deep learning [36] during data acquisition should be further tested to improve the signal to noise ratio of DMI at 3T.
3. Establish reliability and repeatability: At this stage, most DMI experiments carried out are small-scaled animal studies. Animal studies provide the opportunity to better understand fundamental aspects of biochemistry and the effect of gene mutation, therapy, environmental factors on tumour pathology which is unethical to be tested in real patients. These early preclinical feasibility studies should also include tests of repeatability and precision to measure the variability of DMI results. However, ultimately, the most robust evidence for successful clinical implementation of DMI can only be established in human trials on a multi-institutional level. Early clinical trials should validate DMI against an accepted reference standard for safety, tumour characterization, monitoring and standardise the report of adverse events. Later down the line, multicentre clinical trials must be established, and appropriate investigative but pragmatic MR protocols need to be developed.
4. Complementary value with other imaging modalities: Decision about the suitable imaging technique for clinical use depends not purely on the sensitivity or robustness of the method but also the cost effectiveness and accessibility of the imaging tool compared to its potential alternatives. It is plausible that optimal imaging strategy for particular clinical challenge lies with combination of complementary modalities. The availability of ^2H RF coils is still very limited. If only a ^1H coil is available, quantitative exchanged-labelled turnover MRS is a method presented by Rich et al. [37] which enables ^2H glucose be indirectly detected via ^1H MRS. The experimental sensitivity

of non-hyperpolarized ^{13}C MRSI and DMI were compared by de Graaf et al. [34] showing a higher sensitivity for DMI. However, Kaggie et al. [35] suggested that when DMI is compared with hyperpolarized ^{13}C MRSI, ^{13}C MRSI could probe early rapid lactate production, and DMI probe the later slower production of Glx. Therefore, ^{13}C MRSI and DMI could have complementary role in cancer metabolism studies. A comprehensive comparison between different MRS methods concerning the sensitivity of the detection of the different labelled metabolites is still missing and should be addressed in future research studies.

- Radiofrequency detectors for ^2H sensitivity enhancement: One current road blocker and practical obstacle for clinical translation of ^2H MR is the lack of appropriate radiofrequency (RF) MR detectors. This need continues to motivate new research on multi-channel RF arrays which would help to enhance sensitivity and to lower detection thresholds [38–41]. Research directions include anatomically adaptive, lightweight, elastically stretchable or flexible configurations that perfectly conform to the human body to enhance SNR through improving the filling factor. Another area of current intense research is the development of multi-purpose, modular RF receiver arrays, which may eliminate the need for RF coil arrays dedicated to specific anatomy, targets or ^2H DMI/DMS applications. Figure 2 shows an example of a multi-purpose, modular transmit/receive RF array which supports ^2H DMI/DMS. This is an extension of previous developments tailored for ^1H MRI but uses hexagonal building blocks to form an array [42]. Each building block comprises 4 RF elements. It can be driven in the parallel transmission mode but also supports excitation using a single feeding RF channel. For the latter fixed phase settings are used for each element for transmission field (B_1^+) shaping depending on the target anatomy. Phase setting can be conveniently changed and hardware adapted by replacing the phase shifter module of the universal interface which is used to connect the RF array with the MR scanner.

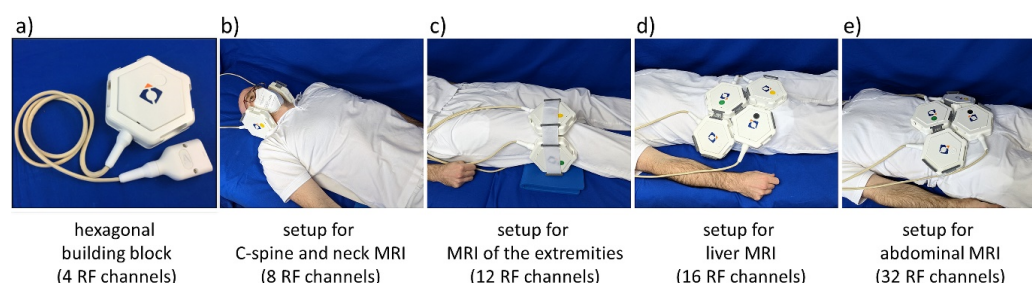


Figure 2. Lightweight and modular Radiofrequency (RF) transceiver array tailored for ^2H MR. This configuration uses a hexagonal building block comprising 4 RF channels. This modular setup is scalable from 4 to 32 RF channels to conform to various target anatomy. Owing to its adaptable and multi-purpose design it supports for example ^2H MR of the C-spine and neck, the musculoskeletal system, the heart, the liver, the spine, and the abdomen. The modular multi-purpose RF array configuration supports translation of ^2H MR from basic research to clinical science and application. It bodes very well to substitute an arsenal of specific RF coils. This approach benefits cost reduction for equipment and maintenance. Images are courtesy of MRI.TOOLS GmbH, Berlin, Germany.

- Extreme field MRI at 14.0 T or 20.0 T: The future of human MRI will not end at 7.0 T and the field is moving apace in this direction. The recent progress of probing the local concentrations of deuterium and other x-nuclei at 7.0 T provides convincing reasons for wide bore magnets with $B_0 \geq 7.0$ T which spurred the installation of a 10.5 T whole-body MR system suitable for body MRI [43]. Physicists, engineers, and pioneers from related disciplines have already taken further steps into the future. This envisions human MR at 14.0 Tesla and at 20.0 Tesla and is an important conceptual leap [44,45]. These fields will span even more of the crucial “resolution gap” in our understanding of cancer biology. Low frequency X-nuclei MR such as ^2H MR would

particularly benefit from the signal-to-noise ratio (SNR) gain at higher magnetic fields because SNR scales supra-linearly with the magnetic field strength [46]. This would help to lower detection levels and reduce scan times. An SNR gain of two would translate into a scan time reduction of a factor of four. The resonance frequency of ^2H at 20.0 T is approximately 131 MHz, which is similar to the resonance frequency of ^1H at a clinical magnetic field strength of 3.0 T. This makes technology established for ^1H MR at 3.0 T ideal candidates to be perfected and fine-tuned for ^2H MR at 20.0 T.

2. Collaborations: From a research perspective, MR physicists, biochemists, biomedical scientists, clinical oncologists, radiologists, engineers, and computer scientists should come together to optimise the utility of DMS and DMI as described above. From a clinical adoption standpoint, opinions from patients, and various stakeholders involved in the multidisciplinary team is essential for the development of a new imaging modality.

6. Conclusions

The development of more sophisticated DMS and DMI workflows is still at an early stage. However, the huge potential of DMI being a robust, readily available method to map the metabolism of tumours non-invasively in 3D should not be overlooked. More technological advancement in the direction of imaging optimisation, RF detector enhancement and increasing field strength is needed. Successful clinical implementation of DMI requires more human study and collaboration between different teams.

Author Contributions: Conceptualization, H.D. and S.A.; writing—original draft preparation, H.D., A.H., S.W., T.N. and S.A.; writing—review and editing, H.D., A.H., S.W., T.N. and S.A. All authors have read and agreed to the published version of the manuscript.

Funding: This research received no external funding.

Conflicts of Interest: Thoralf Niendorf is the founder and CEO of MRI.TOOLS GmbH, Berlin, Germany. But otherwise, there is no other relationship between the company and the manuscript.

References

1. Martinez-Outschoorn, U.E.; Peiris-Pagés, M.; Pestell, P.G.; Sotgia, F.; Lisanti, M.P. Cancer metabolism: A therapeutic perspective. *Nature reviews. Clin. Oncol.* **2017**, *14*, 11–31. [[CrossRef](#)]
2. Sprinz, C.; Altmayer, S.; Zanon, M.; Watte, G.; Irion, K.; Marchiori, E.; Hochegger, B. Effects of blood glucose level on 18F-FDG uptake for PET/CT in normal organs: A systematic review. *PLoS ONE* **2018**, *13*, e0193140. [[CrossRef](#)] [[PubMed](#)]
3. Zhu, A.; Lee, D.; Shim, H. Metabolic positron emission tomography imaging in cancer detection and therapy response. *Semin. Oncol.* **2011**, *38*, 55–69. [[CrossRef](#)] [[PubMed](#)]
4. Burtscher, I.M.; Holtás, S. Proton MR spectroscopy in clinical routine. *J. Magn. Reson. Imaging* **2001**, *13*, 560–567. [[CrossRef](#)] [[PubMed](#)]
5. Ma, J.; Pinho, M.C.; Harrison, C.E.; Chen, J.; Sun, C.; Hackett, E.P.; Liticker, J.; Ratnakar, J.; Reed, G.D.; Chen, A.P.; et al. Dynamic ^{13}C MR spectroscopy as an alternative to imaging for assessing cerebral metabolism using hyperpolarized pyruvate in humans. *Magn. Reson. Med.* **2022**, *87*, 1136–1149. [[CrossRef](#)]
6. Kurhanewicz, J.; Vigneron, D.B.; Ardenkjaer-Larsen, J.H.; Bankson, J.A.; Brindle, K.; Cunningham, C.H.; Gallagher, F.A.; Keshari, K.R.; Kjaer, A.; Laustsen, C.; et al. Hyperpolarized ^{13}C MRI: Path to Clinical Translation in Oncology. *Neoplasia* **2019**, *21*, 1–16. [[CrossRef](#)]
7. De Feyter, H.M.; Behar, K.L.; Corbin, Z.A.; Fulbright, R.K.; Brown, P.B.; McIntyre, S.; Nixon, T.W.; Rothman, D.L.; de Graaf, R.A. Deuterium metabolic imaging (DMI) for MRI-based 3D mapping of metabolism in vivo. *Sci. Adv.* **2018**, *4*, eaat7314. [[CrossRef](#)]
8. Lu, M.; Zhu, X.; Zhang, Y.; Mateescu, G.; Chen, W. Quantitative assessment of brain glucose metabolic rates using in vivo deuterium magnetic resonance spectroscopy. *J. Cereb. Blood Flow Metab.* **2017**, *37*, 3518–3530. [[CrossRef](#)]
9. De Feyter, H.M.; de Graaf, R.A. Deuterium metabolic imaging—Back to the future. *J. Magn. Reson.* **2021**, *326*, 106932. [[CrossRef](#)]
10. Urey, H.C.; Murphy, G.M.; Brickwedde, F.G. A Name and Symbol for H^2 . *J. Chem. Phys.* **2004**, *1*, 512. [[CrossRef](#)]
11. Ackerman, J.J.; Ewy, C.S.; Becker, N.N.; Shalwitz, R.A. Deuterium nuclear magnetic resonance measurements of blood flow and tissue perfusion employing $2\text{H}_2\text{O}$ as a freely diffusible tracer. *Proc. Natl. Acad. Sci. USA* **1987**, *84*, 4099–4102. [[CrossRef](#)] [[PubMed](#)]
12. Müller, S.; Seelig, J. In vivo NMR imaging of deuterium. *J. Magn. Reson.* **1987**, *72*, 456–466. [[CrossRef](#)]
13. Hagemann, R.; Nief, G.; Roth, E. Absolute isotopic scale for deuterium analysis of natural waters. Absolute D/H ratio for SMOW1. *Tellus* **1970**, *22*, 712–715.

14. Al-Rawi, J.M.A.; Behnam, G.Q.; Taha, N.I. Deuterium nuclear magnetic resonance spectroscopy. 1—Larmor frequency ratio, referencing and chemical shift. *Org. Magn. Reson.* **1981**, *16*, 198–201. [[CrossRef](#)]
15. Krebs, H.A. The citric acid cycle and the Szent-Györgyi cycle in pigeon breast muscle. *Biochem. J.* **1940**, *34*, 775–779. [[CrossRef](#)] [[PubMed](#)]
16. Warburg, O.; Wind, F.; Negelein, E. The metabolism of tumors in the body. *J. Gen. Phys.* **1927**, *8*, 519–530. [[CrossRef](#)]
17. Markovic, S.; Roussel, T.; Agemy, L.; Sasson, K.; Preise, D.; Scherz, A.; Frydman, L. Deuterium MRSI characterizations of glucose metabolism in orthotopic pancreatic cancer mouse models. *NMR Biomed.* **2021**, *34*, e4569. [[CrossRef](#)]
18. Peters, D.C.; Markovic, S.; Bao, Q.; Preise, D.; Sasson, K.; Agemy, L.; Scherz, A.; Frydman, L. Improving deuterium metabolic imaging (DMI) signal-to-noise ratio by spectroscopic multi-echo bSSFP: A pancreatic cancer investigation. *Magn. Reson. Med.* **2021**, *86*, 2604–2617. [[CrossRef](#)]
19. Veltien, A.; van Asten, J.; Ravichandran, N.; de Graaf, R.A.; De Feyter, H.M.; Oosterwijk, E.; Heerschap, A. Simultaneous Recording of the Uptake and Conversion of Glucose and Choline in Tumors by Deuterium Metabolic Imaging. *Cancers* **2021**, *13*, 4034. [[CrossRef](#)]
20. Glunde, K.; Bhujwala, Z.M.; Ronen, S.M. Choline metabolism in malignant transformation. *Nat. Rev. Cancer* **2011**, *11*, 835–848. [[CrossRef](#)]
21. Eisenhauer, E.A.; Therasse, P.; Bogaerts, J.; Schwartz, L.H.; Sargent, D.; Ford, R.; Dancey, J.; Arbuck, S.; Gwyther, S.; Mooney, M.; et al. New response evaluation criteria in solid tumours: Revised RECIST guideline (version 1.1). *Eur. J. Cancer.* **2009**, *45*, 228–247. [[CrossRef](#)] [[PubMed](#)]
22. Campbell, A.; Davis, L.M.; Wilkinson, S.K.; Hesketh, R.L. Emerging Functional Imaging Biomarkers of Tumour Responses to Radiotherapy. *Cancers* **2019**, *11*, 131. [[CrossRef](#)] [[PubMed](#)]
23. Hesse, F.; Somai, V.; Kreis, F.; Bulat, F.; Wright, A.J.; Brindle, K.M. Monitoring tumor cell death in murine tumor models using deuterium magnetic resonance spectroscopy and spectroscopic imaging. *Proc. Natl. Acad. Sci. USA* **2021**, *118*, e2014631118. [[CrossRef](#)] [[PubMed](#)]
24. Pérez-Tomás, R.; Pérez-Guillén, I. Lactate in the Tumor Microenvironment: An Essential Molecule in Cancer Progression and Treatment. *Cancers* **2020**, *12*, 3244. [[CrossRef](#)] [[PubMed](#)]
25. Taglang, C.; Batsios, G.; Mukherjee, J.; Tran, M.; Gillespie, A.M.; Hong, D.; Ronen, S.M.; Luchman, H.A.; Pieper, R.O.; Viswanath, P. Deuterium magnetic resonance spectroscopy enables noninvasive metabolic imaging of tumor burden and response to therapy in low-grade gliomas. *Neuro-Oncology* **2022**, *24*, 1101–1112. [[CrossRef](#)] [[PubMed](#)]
26. Hygino da Cruz, L.C.; Rodriguez, I.; Domingues, R.C.; Gasparetto, E.L.; Sorensen, A.G. Pseudoprogression and pseudoresponse: Imaging challenges in the assessment of posttreatment glioma. *AJNR. Am. J. Neuroradiol.* **2011**, *32*, 1978–1985. [[CrossRef](#)]
27. Batsios, G.; Taglang, C.; Tran, M.; Stevers, N.; Barger, C.; Gillespie, A.M.; Ronen, S.M.; Costello, J.F.; Viswanath, P. Deuterium Metabolic Imaging Reports on TERT Expression and Early Response to Therapy in Cancer. *Clin. Cancer Res. Off. J. Am. Assoc. Cancer Res.* **2022**, *28*, 3526–3536. [[CrossRef](#)]
28. O'Connor, J.P.B.; Aboagye, E.O.; Adams, J.E.; Aerts, H.J.W.L.; Barrington, S.F.; Beer, A.J.; Boellaard, R.; Bohndiek, S.; Brady, M.; Brown, G.; et al. Imaging biomarker roadmap for cancer studies. *Nat. Rev. Clin. Oncol.* **2017**, *14*, 169–186. [[CrossRef](#)]
29. McShane, L.M.; Hayes, D.F. Publication of tumor marker research results: The necessity for complete and transparent reporting. *J. Clin. Oncol. Off. J. Am. Soc. Clin. Oncol.* **2012**, *30*, 4223–4232. [[CrossRef](#)]
30. Hirayama, A.; Kami, K.; Sugimoto, M.; Sugawara, M.; Toki, N.; Onozuka, H.; Kinoshita, T.; Saito, N.; Ochiai, A.; Tomita, M.; et al. Quantitative Metabolome Profiling of Colon and Stomach Cancer Microenvironment by Capillary Electrophoresis Time-of-Flight Mass Spectrometry. *Cancer Res.* **2009**, *69*, 4918–4925. [[CrossRef](#)]
31. Ruhm, L.; Avdievich, N.; Ziegs, T.; Nagel, A.M.; De Feyter, H.M.; de Graaf, R.A.; Henning, A. Deuterium metabolic imaging in the human brain at 9.4 Tesla with high spatial and temporal resolution. *Neuroimage* **2021**, *244*, 118639. [[CrossRef](#)] [[PubMed](#)]
32. Pohmann, R.; Speck, O.; Scheffler, K. Signal-to-noise ratio and MR tissue parameters in human brain imaging at 3, 7, and 9.4 tesla using current receive coil arrays. *Magn. Reson. Med.* **2016**, *75*, 801–809. [[CrossRef](#)] [[PubMed](#)]
33. Vaughan, J.T.; Garwood, M.; Collins, C.M.; Liu, W.; DelaBarre, L.; Adriany, G.; Andersen, P.; Merkle, H.; Goebel, R.; Smith, M.; et al. 7T vs. 4T: RF power, homogeneity, and signal-to-noise comparison in head images. *Magn. Reson. Med.* **2001**, *46*, 24–30. [[CrossRef](#)] [[PubMed](#)]
34. de Graaf, R.A.; Hendriks, A.D.; Klomp, D.W.J.; Kumaragamage, C.; Welting, D.; de Castro, C.S.A.; Brown, P.B.; McIntyre, S.; Nixon, T.W.; Prompers, J.J.; et al. On the magnetic field dependence of deuterium metabolic imaging. *NMR Biomed.* **2020**, *33*, e4235. [[CrossRef](#)] [[PubMed](#)]
35. Kaggie, J.D.; Khan, A.S.; Matys, T.; Schulte, R.F.; Locke, M.J.; Grimmer, A.; Frary, A.; Menih, I.H.; Latimer, E.; Graves, M.J.; et al. Deuterium metabolic imaging and hyperpolarized ^{13}C -MRI of the normal human brain at clinical field strength reveals differential cerebral metabolism. *NeuroImage* **2022**, *257*, 119284. [[CrossRef](#)]
36. Dong, S.; Feyter, H.; Graaf, R.; Duncan, J. A Deep Learning Method for Sensitivity Enhancement in Deuterium Metabolic Imaging (DMI). In Proceedings of the 28th Annual Meeting of ISMRM, Singapore, 24 July 2020.
37. Rich, L.J.; Bagga, P.; Wilson, N.E.; Schnall, M.D.; Detre, J.A.; Haris, M.; Reddy, R. ^1H magnetic resonance spectroscopy of ^2H -to- ^1H exchange quantifies the dynamics of cellular metabolism in vivo. *Nat. Biomed. Eng.* **2020**, *4*, 335–342. [[CrossRef](#)]
38. Zhang, B.; Sodickson, D.K.; Cloos, M.A. A high-impedance detector-array glove for magnetic resonance imaging of the hand. *Nat. Biomed. Eng.* **2018**, *2*, 570–577. [[CrossRef](#)]

39. Eigentler, T.W.; Kuehne, A.; Boehmert, L.; Dietrich, S.; Els, A.; Waiczies, H.; Niendorf, T. 32-Channel self-grounded bow-tie transceiver array for cardiac MR at 7.0T. *Magn. Reson. Med.* **2021**, *86*, 2862–2879. [[CrossRef](#)]
40. Gruber, B.; Rehner, R.; Laistler, E.; Zink, S. Anatomically Adaptive Coils for MRI—A 6-Channel Array for Knee Imaging at 1.5 Tesla. *Front. Phys.* **2020**. [[CrossRef](#)]
41. Vincent, J.M.; Gim, M.; Rispoli, J.V. Elastically Stretchable and Flexible RF Receive Coils for Magnetic Resonance Imaging. In Proceedings of the 2021 International Conference on Electromagnetics in Advanced Applications (ICEAA), Honolulu, HI, USA, 9–13 August 2021; p. 319.
42. Graessl, A.; Renz, W.; Hezel, F.; Dieringer, M.A.; Winter, L.; Oezerdem, C.; Rieger, J.; Kellman, P.; Santoro, D.; Lindel, T.D. Modular 32-channel transceiver coil array for cardiac MRI at 7.0T. *Magn. Reson. Med.* **2014**, *72*, 276–290. [[CrossRef](#)]
43. Ertürk, M.A.; Wu, X.; Eryaman, Y.; Van de Moortele, P.; Auerbach, E.J.; Lagore, R.L.; DelaBarre, L.; Vaughan, J.T.; Uğurbil, K.; Adriany, G.; et al. Toward imaging the body at 10.5 tesla. *Magn. Reson. Med.* **2017**, *77*, 434–443. [[CrossRef](#)] [[PubMed](#)]
44. Budinger, T.F.; Bird, M.D.; Frydman, L.; Long, J.R.; Mareci, T.H.; Rooney, W.D.; Rosen, B.; Schenck, J.F.; Schepkin, V.D.; Sherry, D.; et al. Toward 20 T magnetic resonance for human brain studies: Opportunities for discovery and neuroscience rationale. *Magma* **2016**, *29*, 617–639. [[CrossRef](#)] [[PubMed](#)]
45. Winter, L.; Niendorf, T. Electrodynamics and radiofrequency antenna concepts for human magnetic resonance at 23.5 T (1 GHz) and beyond. *Magma* **2016**, *29*, 641–656. [[PubMed](#)]
46. Le Ster, C.; Grant, A.; Van de Moortele, P.; Monreal-Madrigal, A.; Adriany, G.; Vignaud, A.; Mauconduit, F.; Rabrait-Lerman, C.; Poser, B.A.; Ugurbil, K.; et al. Magnetic field strength dependent SNR gain at the center of a spherical phantom and up to 11.7T. *Magn. Reson. Med.* **2022**, *85*, 2131–2138. [[CrossRef](#)] [[PubMed](#)]

Disclaimer/Publisher’s Note: The statements, opinions and data contained in all publications are solely those of the individual author(s) and contributor(s) and not of MDPI and/or the editor(s). MDPI and/or the editor(s) disclaim responsibility for any injury to people or property resulting from any ideas, methods, instructions or products referred to in the content.